IDENTIFICATION OF VISCOELASTIC MATERIALS [1]

M. Mossberg *, **L. Hillström** **, and **T. Söderström** *

* *Dept. of Systems and Control, Information Technology, Uppsala University, P.O. Box 27, SE-751 03 Uppsala, Sweden*
** *Ångström Laboratory, Uppsala University, P.O. Box 534, SE-751 21 Uppsala, Sweden*

Abstract: The frequency-dependent complex modulus for a linearly viscoelastic material is estimated from wave propagation experiments. In these experiments, strains at different sections of a bar specimen are measured as functions of time. The time series are then transformed into the frequency domain, where the identification is made. Two identification techniques, a non-parametric and a parametric, are considered in the paper. Analyses of the quality of the estimates given by the two different techniques are carried out, and approximate expressions for the covariance matrices of the complex modulus are provided. The validity of these expressions are confirmed by numerical studies as well as by real experiments. A comparison between the results of the non-parametric and parametric approaches is made. The results of the comparison are that the parametric model describes the complex modulus quite well and that the variances for the parametric estimates are considerably smaller.

Keywords: Distributed system; Material functions; Non-parametric and parametric identification; Frequency domain data

1. INTRODUCTION

The frequency-dependent complex modulus relates stress and strain of a linearly viscoelastic material. Polymers are examples of materials that can be approximated as linearly viscoelastic. In order to make efficient use of engineering materials with viscoelastic behaviour, it is important to know their complex moduli at relevant frequencies and temperatures.

An experiment as in Fig. 1 is carried out. A bar specimen is axially impacted, and as a result waves start to propagate through the bar. The waves are associated with strains in the material, and from known strains $\varepsilon_1, \varepsilon_2, \ldots, \varepsilon_n$ at sections located at $x_1, x_2, \ldots, x_n$ one can determine the complex modulus. It turns out that it is difficult to obtain estimates of good quality at certain frequencies. It is therefore important to know how the sensors should be placed in order to extract as much information as possible from the known strains.

This problem, and closely related ones, have been studied in earlier papers, see for example Buchanan (1987); Hull (1996); Soula et al. (1997).Other authors have mostly used non-parametric approaches, with Sogabe and Tsuzuki (1986) as an example of an exception. An analysis of the quality of the estimate is lacking in most papers, with Buchanan (1987) as an exception. In this paper a non-parametric and a parametric identification technique are considered. The two methods are analysed and compared using both numerical data and real data from experiments.

[1] Work supported by Swedish Research Council for Engineering Sciences under contracts 96–212 and 98–137.

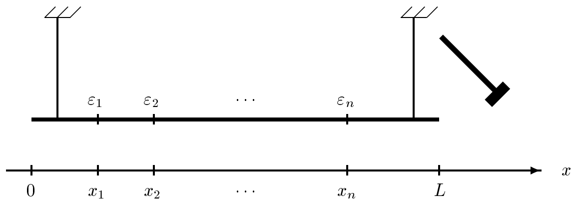

Fig. 1. Experimental set-up.

2. MODEL

The wave propagation in the bar is described by

$$\frac{\partial^2 \hat{\varepsilon}(x,\omega)}{\partial x^2} - \gamma^2(\omega)\hat{\varepsilon}(x,\omega) = 0, \tag{1}$$

where $\hat{\varepsilon}(x,\omega)$ is the Fourier transform of the axial strain $\varepsilon(x,t)$ at section x and time t, ω is the angular frequency, $\gamma(\omega)$ is the wave propagation coefficient which is related to the complex modulus $E(\omega)$ through

$$\gamma^2(\omega) = -\frac{\rho\omega^2}{E(\omega)}, \tag{2}$$

where ρ is the density. For the case of linearly *elastic* materials, such as steel, $E(\omega)$ is real valued and constant (the modulus of elasticity or Young's modulus), and $\gamma(\omega)$ is imaginary valued. The general solution of (1) is

$$\hat{\varepsilon}(x,\omega) = \hat{P}(\omega)e^{-\gamma(\omega)x} + \hat{N}(\omega)e^{\gamma(\omega)x}, \tag{3}$$

where $\hat{P}(\omega)$ and $\hat{N}(\omega)$ are complex valued functions of ω. The boundary conditions

$$\hat{\varepsilon}(0,\omega) = 0, \tag{4}$$
$$\hat{\varepsilon}(L,\omega) = \Phi(\omega) \tag{5}$$

are assumed, where $\Phi(\omega)$ denotes the Fourier transform of the strain pulse generated at the right end of the bar specimen. The boundary condition (4) represents the free left end.

3. A NON-PARAMETRIC IDENTIFICATION TECHNIQUE

3.1 *Description*

Strains $\varepsilon(x_j, t_k)$ are assumed to be at sections x_j, with $j = 1, \ldots, n$, at times $t_k = k\Delta t$, with $k = 1, \ldots, N$, where Δt is the sampling interval and N is the number of samples. After Fourier transformation we get $\hat{\varepsilon}_j(\omega_k) = \hat{\varepsilon}(x_j, \omega_k)$ for frequencies

$$\omega_k = \frac{2\pi k}{N\Delta t}, \qquad k = 1, \ldots, N. \tag{6}$$

From these data, $E(\omega_k)$ are to be determined for every ω_k.

In this section, we will describe a *non-parametric* method for estimating $\gamma(\omega_k)$. When this has been done, $E(\omega_k)$ can be obtained from (2). By using (3), we can form the nonlinear system of equations

$$\mathbf{A}\big(\gamma(\omega_k)\big)\begin{bmatrix}\hat{P}(\omega_k)\\ \hat{N}(\omega_k)\end{bmatrix} = \hat{\varepsilon}(\omega_k), \tag{7}$$

where

$$\mathbf{A}\big(\gamma(\omega_k)\big) = \begin{bmatrix} e^{-\gamma(\omega_k)x_1} & e^{\gamma(\omega_k)x_1} \\ \vdots & \vdots \\ e^{-\gamma(\omega_k)x_n} & e^{\gamma(\omega_k)x_n}\end{bmatrix}, \tag{8}$$

$$\hat{\varepsilon}(\omega_k) = \begin{bmatrix}\hat{\varepsilon}_1(\omega_k) & \cdots & \hat{\varepsilon}_n(\omega_k)\end{bmatrix}^T, \tag{9}$$

for the unknowns $\gamma(\omega_k)$, $\hat{P}(\omega_k)$ and $\hat{N}(\omega_k)$. In order to estimate $\gamma(\omega_k)$, we introduce the loss function

$$U\big(\gamma(\omega_k), \hat{P}(\omega_k), \hat{N}(\omega_k)\big) = \left\| \hat{\varepsilon}(\omega_k) - \mathbf{A}\big(\gamma(\omega_k)\big)\begin{bmatrix}\hat{P}(\omega_k)\\ \hat{N}(\omega_k)\end{bmatrix}\right\|^2, \tag{10}$$

which we wish to minimise with respect to $\gamma(\omega_k)$, $\hat{P}(\omega_k)$ and $\hat{N}(\omega_k)$. Since this is a separable least squares problem, we do this in two steps. In the first step (10) is minimised with respect to $\hat{P}(\omega_k)$ and $\hat{N}(\omega_k)$ for a given $\gamma(\omega_k)$, i.e.,

$$\begin{bmatrix}\hat{P}_{\text{est}}(\omega_k)\\ \hat{N}_{\text{est}}(\omega_k)\end{bmatrix} = \arg\min_{\hat{P}(\omega_k),\hat{N}(\omega_k)} U\big(\gamma(\omega_k), \hat{P}(\omega_k), \hat{N}(\omega_k)\big). \tag{11}$$

The solution of (11) is given by

$$\begin{bmatrix}\hat{P}_{\text{est}}(\omega_k)\\ \hat{N}_{\text{est}}(\omega_k)\end{bmatrix} = \mathbf{A}^\dagger\big(\gamma(\omega_k)\big)\hat{\varepsilon}(\omega_k), \tag{12}$$

where $\mathbf{A}^\dagger = (\mathbf{A}^*\mathbf{A})^{-1}\mathbf{A}^*$ is the pseudoinverse of $\mathbf{A}$. The second step of the minimisation procedure is to consider the concentrated loss function

$$W\big(\gamma(\omega_k)\big) \triangleq U\big(\gamma(\omega_k), \hat{P}_{\text{est}}(\omega_k), \hat{N}_{\text{est}}(\omega_k)\big) = \left\|\hat{\varepsilon}(\omega_k) - \mathbf{A}\big(\gamma(\omega_k)\big)\mathbf{A}^\dagger\big(\gamma(\omega_k)\big)\hat{\varepsilon}(\omega_k)\right\|^2 \tag{13}$$

from which an estimate of the complex valued $\gamma_{\text{est}}(\omega_k)$ is obtained as

$$\gamma_{\text{est}}(\omega_k) = \arg\min_{\gamma(\omega_k)} W\big(\gamma(\omega_k)\big). \tag{14}$$

Finally, when $\gamma_{\text{est}}(\omega_k)$ is obtained, an estimate $E_{\text{est}}(\omega_k)$ can be obtained from (2) as

$$E_{\text{est}}(\omega_k) = -\frac{\rho\omega_k^2}{\gamma_{\text{est}}^2(\omega_k)}. \tag{15}$$

Remark. When $n = 3$, the system of equations (7) has, in the case of equidistantly spaced sensors, one unique and exact solution for $\hat{P}(\omega_k)$, $\hat{N}(\omega_k)$ and $\gamma(\omega_k)$. See Hillström et al. (2000) for an analysis of this case.

3.2 *Accuracy analysis*

We will first derive an asymptotic expression for the accuracy of the estimated wave propagation coefficient (14), which is valid when the signal-to-noise ratio (SNR) tends to infinity. Secondly, we will establish the corresponding expression for the complex modulus. To be more specific, a vector $\varepsilon(t_k)$ of measured strains at time t_k is assumed to equal a vector $\boldsymbol{\epsilon}(t_k)$ of *true* and *unknown* strains plus a stochastic disturbance $\mathbf{v}(t_k)$,

$$\varepsilon(t_k) = \boldsymbol{\epsilon}(t_k) + \mathbf{v}(t_k). \tag{16}$$

Our analysis covers the case when the noise $\mathbf{v}(t_k)$ is small in comparison to $\boldsymbol{\epsilon}(t_k)$, but nonnegligible.

For the loss function $W\big(\gamma(\omega_k)\big)$ given by (13) it holds that $W\big(\gamma(\omega_k)\big) : \mathbb{C} \to \mathbb{R}$. If we instead consider $W\big(\gamma(\omega_k)\big) = V\big(\mathbf{g}(\omega_k)\big)$, where the elements of the vector

$$\mathbf{g}(\omega_k) = \big[\gamma_r(\omega_k)\ \ \gamma_i(\omega_k)\big]^T \tag{17}$$

are the real and imaginary parts of $\gamma(\omega_k)$, it holds that $V\big(\mathbf{g}(\omega_k)\big) : \mathbb{R}^2 \to \mathbb{R}$. This means that we can use only real valued variables in the analysis.

Since $\mathbf{g}_{\text{est}}(\omega_k)$ minimises $V\big(\mathbf{g}(\omega_k)\big)$ and thereby (13), we have that

$$\mathbf{V}'\big(\mathbf{g}_{\text{est}}(\omega_k)\big) = \mathbf{0}, \tag{18}$$

where $\mathbf{V}'\big(\mathbf{g}(\omega_k)\big)$ is the gradient vector of $V\big(\mathbf{g}(\omega_k)\big)$. Assume that the estimated wave propagation coefficient converges to

$$\mathbf{g}_\infty(\omega_k) = \lim_{\text{SNR}\to\infty} \mathbf{g}_{\text{est}}(\omega_k), \tag{19}$$

as the SNR tends to infinity. Next, we make a Taylor series expansion around $\mathbf{g}_\infty(\omega_k)$ under the assumption that the SNR is large and obtain

$$\begin{aligned}\mathbf{0} = \mathbf{V}'\big(\mathbf{g}_{\text{est}}(\omega_k)\big) &= \mathbf{V}'\big(\mathbf{g}_\infty(\omega_k)\big) \\ &+ \mathbf{V}''\big(\mathbf{g}_\infty(\omega_k)\big)\big(\mathbf{g}_{\text{est}}(\omega_k) - \mathbf{g}_\infty(\omega_k)\big) + \dots ,\end{aligned} \tag{20}$$

where $\mathbf{V}''\big(\mathbf{g}(\omega_k)\big)$ is the Hessian matrix of $V\big(\mathbf{g}(\omega_k)\big)$. This gives

$$\begin{aligned}\tilde{\mathbf{g}}(\omega_k) &\triangleq \mathbf{g}_{\text{est}}(\omega_k) - \mathbf{g}_\infty(\omega_k) \\ &\approx -\big[\mathbf{V}''\big(\mathbf{g}_\infty(\omega_k)\big)\big]^{-1}\mathbf{V}'\big(\mathbf{g}_\infty(\omega_k)\big).\end{aligned} \tag{21}$$

We also assume that

$$\lim_{\text{SNR}\to\infty} \mathbf{V}''\big(\mathbf{g}_\infty(\omega_k)\big) = \mathbf{H}(\omega_k), \tag{22}$$

where $\mathbf{H}(\omega_k) > \mathbf{0}$ is a positive definite matrix. The following result can now be given:

Result 1. The correlation between the estimation errors of the wave propagation coefficient at frequencies ω_a and ω_b can be described through

$$\mathrm{E}\{\tilde{\mathbf{g}}(\omega_a)\tilde{\mathbf{g}}^T(\omega_b)\} \approx \mathbf{H}^{-1}(\omega_a)\mathbf{G}(\omega_a,\omega_b)\mathbf{H}^{-T}(\omega_b), \tag{23}$$

where

$$\mathbf{G}(\omega_a,\omega_b) = \mathrm{E}\Big\{\mathbf{V}'\big(\mathbf{g}_\infty(\omega_a)\big)\big[\mathbf{V}'\big(\mathbf{g}_\infty(\omega_b)\big)\big]^T\Big\}. \tag{24}$$

Explicit expressions for $\mathbf{H}(\omega_k)$ and $\mathbf{G}(\omega_a,\omega_b)$ are derived in Mossberg et al.

When the wave propagation coefficient $\gamma(\omega_k)$ is known, the complex modulus $E(\omega_k)$ can be obtained from (2). Let

$$\mathbf{e}(\omega_k) = \big[E_r(\omega_k)\ \ E_i(\omega_k)\big]^T, \tag{25}$$

where $E_r(\omega_k)$ and $E_i(\omega_k)$ denote the real and imaginary parts of $E(\omega_k)$, and rewrite (2) as

$$\mathbf{e}(\omega_k) = \mathbf{f}\big(\mathbf{g}(\omega_k)\big), \tag{26}$$

where $\mathbf{f}\big(\mathbf{g}(\omega_k)\big) : \mathbb{R}^2 \to \mathbb{R}^2$. Using the so called Gauss approximation, we have

Result 2. The correlation between the estimation errors of the complex modulus at frequencies ω_a and ω_b can be described through

$$\begin{aligned}&\mathrm{E}\{\tilde{\mathbf{e}}(\omega_a)\tilde{\mathbf{e}}^T(\omega_b)\} \\ &\approx \begin{cases}\mathbf{0} & \text{if } a \neq b, \\ \mathbf{F_g}\mathrm{E}\{\tilde{\mathbf{g}}(\omega_a)\tilde{\mathbf{g}}^T(\omega_a)\}\mathbf{F_g}^T & \text{if } a = b,\end{cases}\end{aligned} \tag{27}$$

where

$$\mathbf{F_g} = \frac{\partial\mathbf{f}\big(\mathbf{g}(\omega_a)\big)}{\partial\mathbf{g}(\omega_a)}. \tag{28}$$

4. A PARAMETRIC IDENTIFICATION TECHNIQUE

4.1 *Description*

The standard linear solid model Zener (1948) in Fig. 2 is a commonly used parametric model for the complex modulus. The model has two springs and one dashpot and is useful for low to moderately high frequencies. The complex modulus

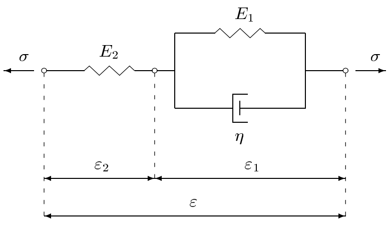

Fig. 2. The standard linear solid model.

given by the model is

$$E(\omega,\boldsymbol{\theta}) = \frac{E_2(E_1 + \mathrm{i}\omega\eta)}{E_1 + E_2 + \mathrm{i}\omega\eta}, \tag{29}$$

where the model parameter is

$$\boldsymbol{\theta} = (E_1, E_2, \eta)^T. \tag{30}$$

Assume that the material can be described by the standard linear solid model. Then, as a consequence

$$E(\omega_k) = E(\omega_k,\boldsymbol{\theta}_0) + \tilde{E}(\omega_k), \tag{31}$$

where $\boldsymbol{\theta}_0$ is the true parameter vector and $\tilde{E}(\omega_k)$ is a stochastic disturbance. This means that we assume that the material can be described by the standard linear solid model and that the true and unknown strains in (16) depend on $\boldsymbol{\theta}_0$. We introduce the loss function

$$\begin{aligned} J(\boldsymbol{\theta}) &= \sum_{k=1}^{N} \left\| \begin{bmatrix} E_r(\omega_k) \\ E_i(\omega_k) \end{bmatrix} - \begin{bmatrix} E_r(\omega_k, \boldsymbol{\theta}) \\ E_i(\omega_k, \boldsymbol{\theta}) \end{bmatrix} \right\|^2_{\mathbf{C}(\omega_k)} \\ &= \sum_{k=1}^{N} \Big\{ \big(E_r(\omega_k) - E_r(\omega_k, \boldsymbol{\theta})\big)^2 \mathbf{C}_{11}(\omega_k) \\ &\quad + 2\big(E_r(\omega_k) - E_r(\omega_k, \boldsymbol{\theta})\big) \\ &\qquad \times \big(E_i(\omega_k) - E_i(\omega_k, \boldsymbol{\theta})\big) \mathbf{C}_{12}(\omega_k) \\ &\quad + \big(E_i(\omega_k) - E_i(\omega_k, \boldsymbol{\theta})\big)^2 \mathbf{C}_{22}(\omega_k) \Big\}, \end{aligned} \tag{32}$$

where the weighting matrix is chosen as

$$\mathbf{C}(\omega_k) \triangleq \big[\mathbf{K}(\omega_k)\big]^{-1}, \tag{33}$$

with

$$\mathbf{K}(\omega_k) \triangleq \mathrm{E}\{\tilde{\mathbf{e}}(\omega_k)\tilde{\mathbf{e}}^T(\omega_k)\} \tag{34}$$

given by (27). An estimate $\boldsymbol{\theta}_{\text{est}}$ is obtained from (32) as

$$\boldsymbol{\theta}_{\text{est}} = \arg\min_{\boldsymbol{\theta}} J(\boldsymbol{\theta}). \tag{35}$$

An alternative is to consider a loss function where the strains or the Fourier transformed strains are used directly.

4.2 *Accuracy analysis*

In this section we will derive an asymptotic expression for the accuracy of the estimated parameter vector (35) and the associated complex modulus. We will make the same assumptions and apply the same technique as in Section 3.2.

From a Taylor series expansion around

$$\boldsymbol{\theta}_0 = \lim_{\text{SNR}\to\infty} \boldsymbol{\theta}_{\text{est}} \tag{36}$$

we get

$$\tilde{\boldsymbol{\theta}} \triangleq \boldsymbol{\theta}_{\text{est}} - \boldsymbol{\theta}_0 \approx -\big[\mathbf{J}''(\boldsymbol{\theta}_0)\big]^{-1}\mathbf{J}'(\boldsymbol{\theta}_0). \tag{37}$$

We also assume that

$$\lim_{\text{SNR}\to\infty} \mathbf{J}''(\boldsymbol{\theta}_0) = \boldsymbol{\mathcal{H}}, \tag{38}$$

where $\boldsymbol{\mathcal{H}} > 0$ is a positive definite matrix. The following result can now be given:

Result 3. The correlation between the estimation errors of the parameter vector $\boldsymbol{\theta}$ of the standard linear solid model can be described through

$$\mathrm{E}\{\tilde{\boldsymbol{\theta}}\tilde{\boldsymbol{\theta}}^T\} \approx \boldsymbol{\mathcal{H}}^{-1}\boldsymbol{\mathcal{G}}\boldsymbol{\mathcal{H}}^{-T}, \tag{39}$$

where

$$\boldsymbol{\mathcal{G}} = \mathrm{E}\Big\{\mathbf{J}'(\boldsymbol{\theta}_0)\big[\mathbf{J}'(\boldsymbol{\theta}_0)\big]^T\Big\}. \tag{40}$$

The correlation between the estimation errors of the complex modulus can be obtained by linearisation. Let

$$\mathbf{e}(\omega_k, \boldsymbol{\theta}) = \big[E_r(\omega_k, \boldsymbol{\theta})\;\; E_i(\omega_k, \boldsymbol{\theta})\big]^T \tag{41}$$

and write (29) as

$$\mathbf{e}(\omega_k, \boldsymbol{\theta}) = \mathbf{f}(\omega_k, \boldsymbol{\theta}), \tag{42}$$

where $\mathbf{f}(\omega_k, \boldsymbol{\theta}) : \mathbb{R}^3 \to \mathbb{R}^2$.

Result 4. The correlation between the estimation errors of the complex modulus at frequencies ω_a and ω_b can be described through

$$\begin{aligned} &\mathrm{E}\{\tilde{\mathbf{e}}(\omega_a, \boldsymbol{\theta})\tilde{\mathbf{e}}^T(\omega_b, \boldsymbol{\theta})\} \\ &\qquad \approx \frac{\partial \mathbf{f}(\omega_a, \boldsymbol{\theta})}{\partial \boldsymbol{\theta}} \mathrm{E}\{\tilde{\boldsymbol{\theta}}\tilde{\boldsymbol{\theta}}^T\} \left[\frac{\partial \mathbf{f}(\omega_b, \boldsymbol{\theta})}{\partial \boldsymbol{\theta}}\right]^T. \end{aligned} \tag{43}$$

5. NUMERICAL EXAMPLES

The experiment described in Section 1, the non-parametric identification in Section 3 and the parametric identification in Section 4 were considered in Monte Carlo simulations in order to investigate the validity of expressions (27) of Result 2 and (43) of Result 4. Data for the wave propagation coefficient were generated from the standard linear solid model. The Fourier transformed strains were then obtained from (3).

Since the measurements of the strains are made in the time domain and are affected by noise as in (16), the Fourier transformed strains were inversely transformed to the time domain where noise was added. The procedure of adding noise to the time domain data, transforming the data to the frequency domain and making an estimation was repeated 100 times for different noise realisations with variance $\sigma^2 = 1 \cdot 10^{-18}$. The maximum absolute value of the true strain $\epsilon_j(t_k)$ was of order 6 μm/m. The length of the bar was $L = 2$ m, the number of data $N = 20\,001$ and the sampling interval $\Delta t = 10$ μs. The strain pulse $\Phi(\omega)$ at the right end of the bar was chosen so that a sufficient excitation for all considered frequencies was obtained. Moreover, the parameters in the standard linear solid model were

$$\boldsymbol{\theta}_0 = (56\,\text{GPa}, 5.6\,\text{GPa}, 2\,\text{MPa}\cdot\text{s})^T. \tag{44}$$

With this choice of the viscoelastic parameters, the standard linear solid model applies to the dynamic behavior of PMMA (plexiglass), a material with density $\rho = 1180\,\text{kg/m}^3$. The locations of the sections were $x = \{0, 0.290, 0.646, 1.078, 1.600\}$ m, i.e., the free end was used and we know that the strains are zero there. However, noise was added also to the free end strains.

The standard deviations of the estimates from the 100 simulated experiments were then compared to the ones given by the square roots of the diagonal elements in (27) and (43). The results of the comparisons are shown in Fig. 3. The theoretical expressions for the expected accuracy of the non-parametric and parametric methods are clearly confirmed by the numerical studies.

We see that it is possible to obtain a model that perfectly describes the result of the non-parametric identification. This is of course expected since data were generated from the model. The standard deviations for the parametric estimates are about 100 times smaller than for the non-parametric estimates.

6. EXPERIMENTS

In the previous section we saw that (27) and (43) were confirmed when simulated data were used. Naturally, it is even more important to find out if the theoretical expressions are applicable also when real data are used. Therefore, ten experiments, as identical as possible, were carried out with a bar specimen made of plexiglass. Additional information about the experiments can be found in Hillström et al. (2000). The standard deviations from the ten experiments were compared with the ones from the theoretical expressions. The locations of the sensors and the length of the bar were the same as in the numerical example of Section 5. The number of data points were $N = 4096$ and the sampling interval $\Delta t = 20$ μs. The variance of the measurement noise was estimated to $\sigma^2 \approx 3.6 \cdot 10^{-14}$. To compensate for the noise-free data from the the free end, it was found that $\sigma^2 \approx 2.1 \cdot 10^{-14}$ is a suitable value.

The results of the comparisons are shown in Fig. 4. The theoretical expression describes the experimental standard deviations with high enough accuracy for the non-parametric method. For the parametric method, however, the theoretical expression gives somewhat low values. One reason for this might be that the model does not describe the properties of the material perfectly. Moreover, there is an uncertainty in the estimates of the standard deviations, since they are based on only ten data series.

The identified model describes the result of the non-parametric identification reasonably well. This means that the standard linear solid model is quite useful for describing the properties of the material. It is also possible to have several standard linear solids in series or in parallel, Casula and Carcione (1992); Liu et al. (1976), to get a more complex model that is likely to describe the material even better. Finally, we see that the standard deviations for the parametric estimates are about 100 times smaller than for the non-parametric estimates, which was the case also in the numerical study.

7. CONCLUSIONS

It is of great importance to be able to fully characterise materials with viscoelastic behaviour in order to use them in engineering applications. Both a non-parametric and a parametric identification method of the frequency dependent complex modulus were considered. Asymptotic expressions for the accuracy of the estimated complex modulus, valid for high SNR's, were derived. The validity of the expressions were confirmed by Monte Carlo simulations. Data were also taken from real experiments and it was concluded that the theoretical expressions can describe the experimental standard deviations with high accuracy. It was seen that the standard linear solid model is able to describe the complex modulus quite well and that the standard deviations for the parametric estimates are considerably smaller than for the non-parametric estimates. Other variants of parametric identification are under investigation, such as different criteria functions, more complex model structures and time domain data.

References

J. L. Buchanan. Numerical solution for the dynamic moduli of a viscoelastic bar. *J. Acoust. Soc. Am.*, 81(6):1775–1786, June 1987.

G. Casula and J. M. Carcione. Generalized mechanical model analogies of linear viscoelastic behaviour. *Bollettino Di Geofisica Teorica Ed Applicata*, 34(136):235–256, December 1992.

L. Hillström, M. Mossberg, and B. Lundberg. Identification of complex modulus from measured strains on an axially impacted bar using least squares. To be published in *Journal of Sound and Vibration*, March 2000.

A. J. Hull. An inverse method to measure the axial modulus of composite materials under tension. *Journal of Sound and Vibration*, 195(4):545–551, 1996.

H. Liu, D. L. Anderson, and H. Kanamori. Velocity dispersion due to anelasticity; implications for seismology and mantle composition. *Geophys. J. R. Astr. Soc.*, 47:41–58, 1976.

M. Mossberg, L. Hillström, and T. Söderström. Non-parametric identification of viscoelastic materials from wave propagation experiments. Submitted to *Automatica*.

Y. Sogabe and M. Tsuzuki. Identification of the dynamic properties of linear viscoelastic materials by the wave propagation testing. *Bulletin of JSME*, 29(254):2410–2417, August 1986.

M. Soula, T. Vinh, Y. Chevalier, T. Beda, and C. Esteoule. Measurements of isothermal complex moduli of viscoelastic materials over a large range of frequencies. *Journal of Sound and Vibration*, 205(2):167–184, 1997.

C. Zener. *Elasticity and Anelasticity of Metals.* University of Chicago Press, IL, USA, 1948.

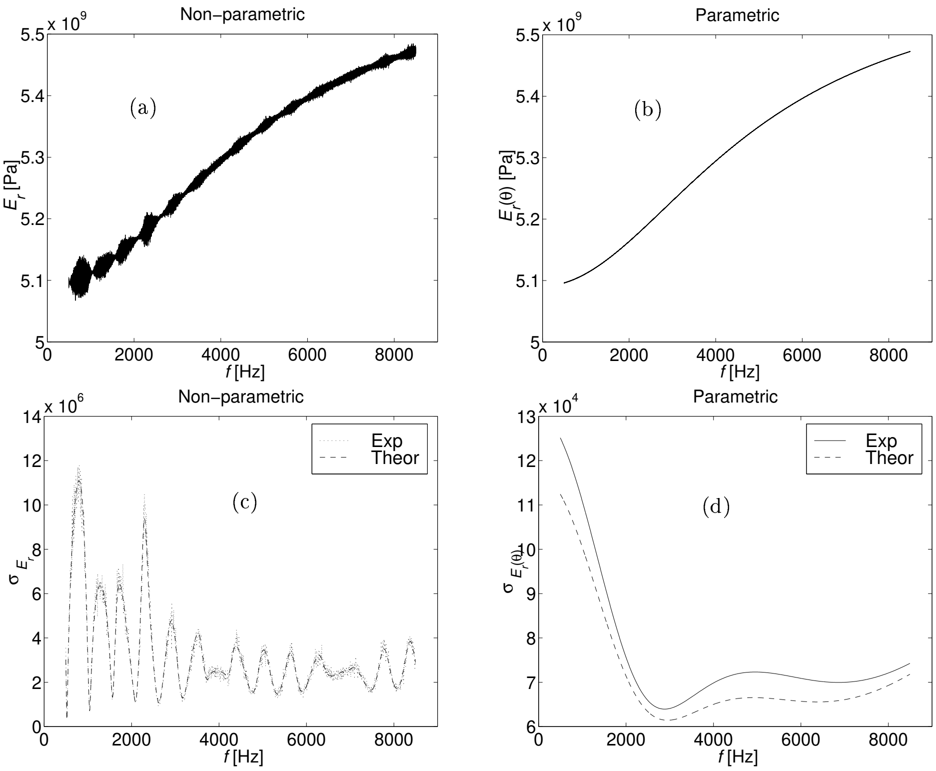

Fig. 3. Monte Carlo simulations. (a) The 100 non-parametric estimates of E_r. (b) The 100 parametric estimates of $E_r(\boldsymbol{\theta})$. (c)–(d) Numerical and theoretical standard deviations for E_r and $E_r(\boldsymbol{\theta})$. Note the different scales. The corresponding results for the imaginary parts are similar.

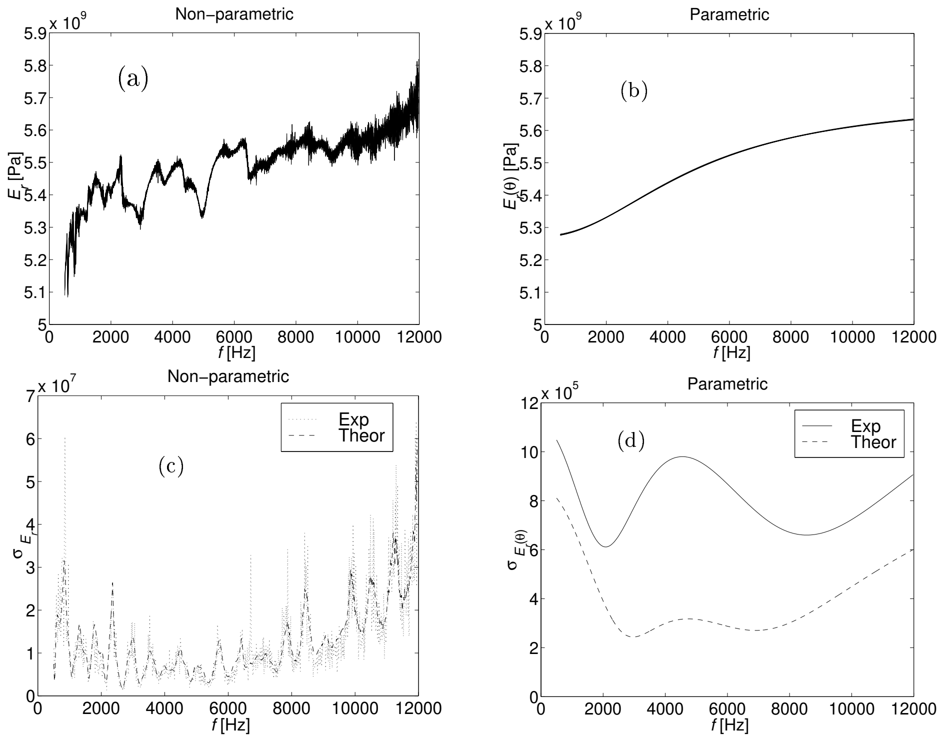

Fig. 4. Experimental data. (a) The 10 non-parametric estimates of E_r. (b) The 10 parametric estimates of $E_r(\boldsymbol{\theta})$. (c)–(d) Experimental and theoretical standard deviations for E_r and $E_r(\boldsymbol{\theta})$. The corresponding results for the imaginary parts are similar.